Applied Physics Letters

RESEARCH ARTICLE | SEPTEMBER 04 2025

Geometry-engineered spring-shaped silicon nanowires for directional airflow sensing on flexible substrates

Zongguang Liu ; Haotian Wu ; Hongyu Wu; Ruijin Hu ; Shaobo Zhang; Yunqing Cao ; Junzhuan Wang ; Kunji Chen ; Jianmei Chen ; Linwei Yu

Check for updates

Appl. Phys. Lett. 127, 092109 (2025)
https://doi.org/10.1063/5.0283844

View Online
Export Citation

Articles You May Be Interested In

Design of an array of piezoresistive airflow sensors based on pressure loading mode for simultaneous detection of airflow velocity and direction

Rev. Sci. Instrum. (February 2022)

A perspective on ultralong silicon nanowires for flexible sensors

Appl. Phys. Lett. (March 2022)

Calibration method for flap structure of macrofluidic airflow sensor

AIP Conf. Proc. (June 2023)

04 November 2026 08:20:43

Nanotechnology & Materials Science
Optics & Photonics
Impedance Analysis
Scanning Probe Microscopy
Sensors
Failure Analysis & Semiconductors

Unlock the Full Spectrum.
From DC to 8.5 GHz.



Zurich Instruments

Find out more

AIP Publishing

Applied Physics Letters ARTICLE pubs.aip.org/aip/apl

Geometry-engineered spring-shaped silicon nanowires for directional airflow sensing on flexible substrates

Cite as: Appl. Phys. Lett. **127**, 092109 (2025); doi: 10.1063/5.0283844
Submitted: 3 June 2025 · Accepted: 12 August 2025 ·
Published Online: 4 September 2025

View Online Export Citation CrossMark

Zongguang Liu,[1,a)] Haotian Wu,[1] Hongyu Wu,[1] Ruijin Hu,[1] Shaobo Zhang,[1] Yunqing Cao,[1] Junzhuan Wang,[2] Kunji Chen,[2] Jianmei Chen,[3,a)] and Linwei Yu[2,a)]

AFFILIATIONS

[1]College of Physics Science and Technology/Microelectronics Industry Research Institute, Yangzhou University, 225009 Yangzhou, China
[2]School of Electronic Science and Engineering/National Laboratory of Solid-State Microstructures, Nanjing University, 210023 Nanjing, China
[3]Jiangsu Key Laboratory of Integrated Traditional Chinese and Western Medicine for Prevention and Treatment of Senile Diseases, Institute of Translational Medicine, School of Medicine, Yangzhou University, 225001 Yangzhou, China

[a)]**Authors to whom correspondence should be addressed:** zgliu@yzu.edu.cn; cjm@yzu.edu.cn; and yulinwei@nju.edu.cn

ABSTRACT

Precise detection of gentle airflow remains challenging for wearable sensors due to low flexibility and limited directional sensitivity in conventional nanowire designs. Inspired by mechanosensory hairs in human skin, we report a flexible, geometry-engineered airflow sensor based on suspended spring-shaped silicon nanowires (SiNWs), synthesized via an in-plane solid–liquid–solid strategy. The spring-shaped architecture is rationally designed to enhance axial compliance and mechanical resilience, significantly outperforming straight SiNWs under airflow-induced strain, as validated by finite element simulations and mechanical testing. The sensor demonstrates a rapid response time of 80 ms and a linear electrical output in response to gentle airflow ranging from 0.5 to 3 m/s under bending conditions. Notably, its unique structural anisotropy enables directional sensing at 0°, 45°, and 90°, with distinct current responses of 56%, 38%, and 16%, respectively. This work highlights geometry engineering as an effective strategy for enabling directional airflow detection in flexible nanowire-based systems.

Published under an exclusive license by AIP Publishing. https://doi.org/10.1063/5.0283844

04 November 2026 08:20:43

Airflow sensors are in high demand across diverse fields, including aerospace, environmental monitoring, human–machine interfaces, and health monitoring.[1–4] The advent of intelligent systems has heightened interest in sensors that offer high sensitivity, fast response, and directional detection capabilities. In particular, gentle airflow in the range of 0.2–6 m/s provides critical information for applications such as exhalation monitoring and artificial robotics.[5–8] Various film-based airflow sensors have been developed, exploiting thermal, piezoresistive, piezoelectric, triboelectric, and optoelectromechanical effects.[9–11] Despite notable progress, many of these sensors still suffer from slow response times (typically 100 ms to several seconds) and limited multidirectional detection capabilities.[9,12–16]

Inspired by the sensory hairs on human skin and the filiform hairs of insects, both of which are capable of detecting subtle environmental cues, recent research has focused on freestanding vertical one-dimensional (1D) micro/nanomaterial arrays, such as carbon nanotubes,[17] carbon fiber,[18] graphene fibers,[19] as promising candidates for next-generation airflow sensors. These structures offer high surface-to-volume ratios and low inertia, making them highly responsive to external stimuli. Additionally, bridge-type suspended configurations have been proposed to further enhance sensing performance by allowing greater deformation under airflow-induced forces.[10,20] In these configurations, nanowire channels are anchored at both ends while remaining suspended in the central region, enabling substrate-free deformation that leads to measurable changes in current under bias.

Among various 1D materials, silicon nanowires (SiNWs) have emerged as attractive sensing elements due to their pronounced piezoresistive effects and excellent electrical and mechanical properties.[21] The strain-induced modulation of carrier mobility and surface charge distribution in SiNWs enables sensitive and reliable resistance changes under mechanical deformation,[22] making them highly suitable for respiratory monitoring, airflow sensing, and biomechanical signal detection.[23–25]

Published under an exclusive license by AIP Publishing

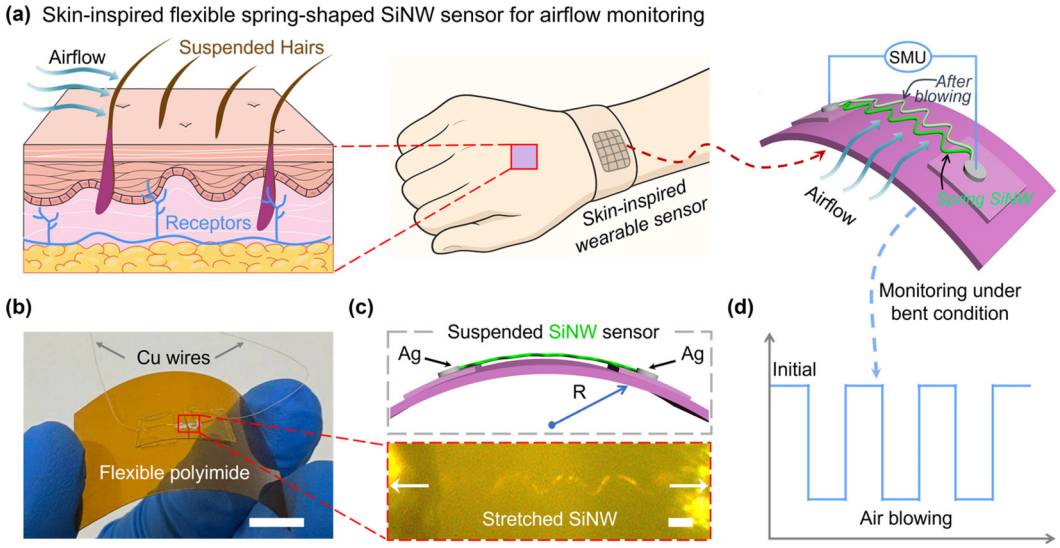


FIG. 1. Design of a flexible, bioinspired SiNW strain sensor for airflow detection. (a) Schematic illustration of the flexible sensor inspired by human skin, featuring a suspended spring-shaped SiNW that responds to airflow via deformation-induced resistance changes. (b) Optical image of the fabricated sensor on a flexible PI substrate. (c) Cross-sectional view of the device showing the suspended, stretchable SiNW bridging two PI pads. (d) Schematic of the airflow-induced deformation mechanism and corresponding resistance variation. The scale bars in (b) and (c) represent 1 cm and 10 μm, respectively.

The advancement of flexible electronics has further expanded the potential of integrating SiNWs into sensors designed for dynamic and deformable environments. Applications such as wearable health monitoring, soft robotics, and environmental sensing require sensors capable of withstanding significant mechanical deformation without compromising performance. However, traditional SiNW-based strain sensors, typically composed of straight nanowires,[26,27] exhibit limited mechanical compliance and are prone to fracture under axial strain, restricting their application in stretchable or highly flexible systems.

To address these challenges, geometric redesign strategy has emerged as a transformative solution for robust strain-sensing applications. Spring-like or serpentine geometries allow SiNWs to accommodate larger strains while maintaining structural integrity. Two primary fabrication strategies have been reported: (1) top-down patterning on silicon-on-insulator wafers via electron-beam lithography followed by anisotropic etching,[28] which offers precise control but suffers from high cost and poor scalability; (2) prestrain-based reconfiguration, in which straight vapor–liquid–solid (VLS) SiNWs are transferred onto pre-stretched elastomeric substrates, and upon relaxation, adopt spring-like geometries.[29–32] However, this method results in substrate-supported structures and is incompatible with suspended configurations essential for high-sensitivity detection.

In our previous work, we developed an in-plane solid–liquid–solid (IPSLS) growth method for fabricating spring-shaped SiNWs.[33–35] In this approach, indium (In) catalyst droplets migrate along lithographically defined spring-shaped edges while absorbing amorphous silicon precursors, yielding well-aligned, crystalline SiNW arrays with elastic geometries. These as-grown SiNWs have demonstrated excellent flexibility and gauge factors in previous applications such as finger motion monitoring.[34,36]

In this work, we present a bioinspired flexible strain sensor based on suspended spring-shaped SiNWs, mimicking the structure and function of biological sensory hairs [Fig. 1(a)]. The spring-shaped SiNWs are precisely transferred using a tapered optical fiber and suspended between two polyimide (PI) pads adhered to a flexible PI substrate [Fig. 1(b)]. Upon substrate bending, the suspended SiNWs remain elevated due to their clamped configuration between two PI pads, which mechanically isolate them from the substrate and minimize strain transfer [Fig. 1(c)]. When exposed to lateral airflow, the suspended structure undergoes additional deformation, resulting in a change in resistance and a measurable current response. The suspended configuration is essential for achieving high airflow sensitivity and directionality, due to its superior mechanical compliance and capacity for out-of-plane deformation, which are severely limited in substrate-supported structures. This architecture enables real-time, directional airflow detection with high sensitivity and mechanical robustness [Fig. 1(d)]. Electrical contacts are formed using silver paste and copper wires, and measurements are conducted using a standard source meter.

The elastic SiNW arrays were synthesized using IPSLS growth strategy,[37,38] as illustrated in Figs. 2(a)–2(c). First, spring-shaped guiding edge patterns were defined on silicon substrates via photolithography followed by inductively coupled plasma (ICP) etching. Indium (In) catalyst pads were subsequently deposited through a sequence of photolithography, thermal evaporation, and liftoff steps [Fig. 2(a)]. The substrates were then loaded into a plasma-enhanced chemical vapor deposition (PECVD) chamber. A brief hydrogen plasma treatment was employed to remove native oxides on the In surface, enabling the formation of discrete molten droplets. Subsequently, a thin film of amorphous silicon (a-Si) was deposited at 150 °C (below the melting point of In) as the precursor layer [Fig. 2(b)]. Raising the substrate temperature to 350 °C caused the In droplets to remelt and migrate along the predefined spring-shaped guiding edges, continuously consuming the a-Si from the vertical sidewalls and forming

04 November 2026 08:20:43

Published under an exclusive license by AIP Publishing

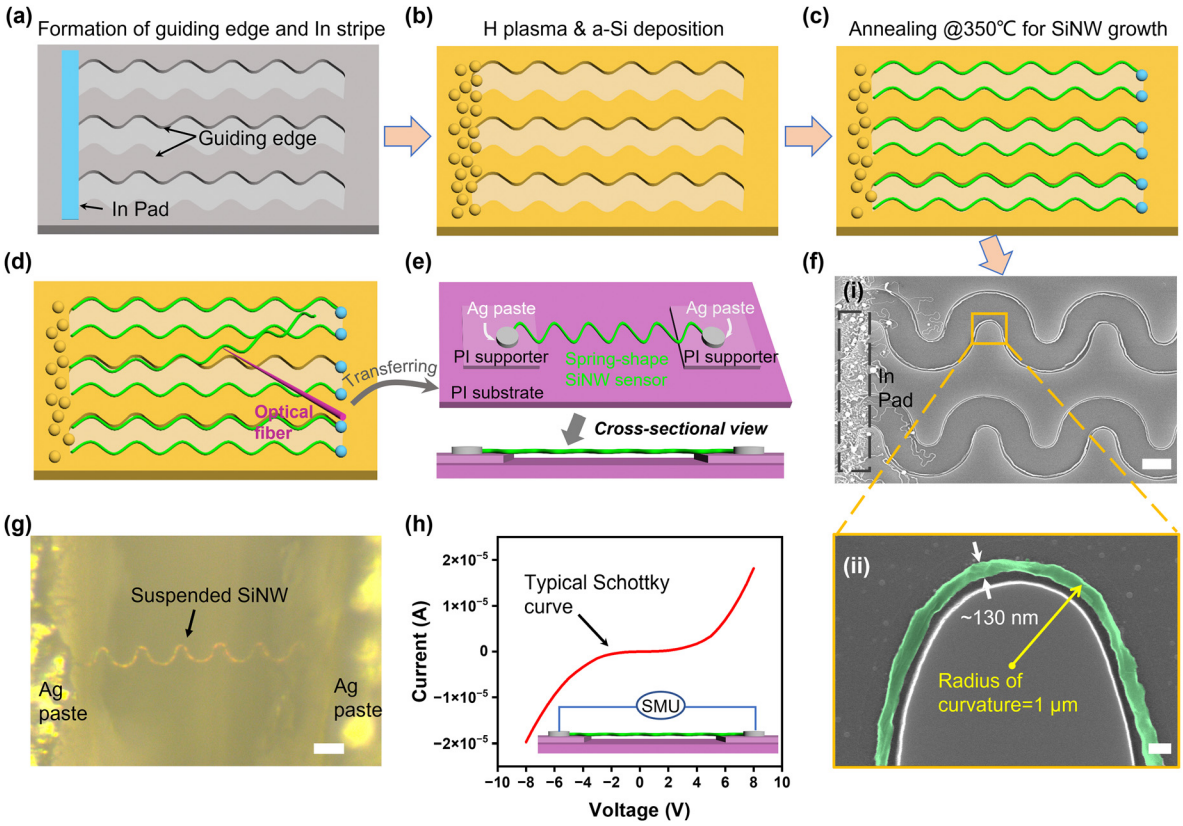


FIG. 2. Fabrication and characterization of the suspended spring-shaped SiNW sensor. (a)–(c) Schematic illustration of spring-shaped SiNW growth via IPSLS method. (d) Illustration of an individual SiNW being picked up using a fine-tipped optical fiber. (e) Schematic of the suspended SiNW sensor configuration. (f) SEM images of the grown spring-shaped SiNW. (g) Optical image of the fabricated sensor showing the suspended SiNW bridging two PI pads. (h) Current–voltage (I–V) characteristics of the sensor, exhibiting back-to-back Schottky diode behavior. Inset shows the measurement setup. The scale bars in (i) and (ii) in (f) represent 3 μm and 200 nm, respectively, and the scale bar in (g) is 10 μm.

well-aligned, spring-shaped crystalline SiNW arrays [Fig. 2(c)]. The resulting SiNWs exhibited a uniform diameter of approximately 130 nm and a curvature radius of ~1 μm [Fig. 2(f)], demonstrating excellent control over structural geometry.

After growth, individual SiNWs were carefully transferred onto a flexible PI substrate using a fine-tipped (~200 nm) optical fiber [Figs. 2(d) and 2(e)]. The nanowires were suspended between two PI support pads to form bridge-like configurations [Fig. 2(g)], which is essential for enabling elastic deformation during airflow sensing. Electrical measurements of the suspended SiNW sensors revealed a typical back-to-back Schottky barrier behavior at the silver paste contacts [Fig. 2(h)], consistent with previous studies, which can be attributed to p-type doping from incorporated In atoms, yielding a doping concentration of $\sim 5 \times 10^{18}$ cm^{-3}.[39,40] The resistance of a suspended spring-shaped SiNW was approximately 2.5 MΩ, and the sensor delivered electrical currents up to 20 μA under a ±8 V bias.

To evaluate the mechanical flexibility and stretchability of the suspended SiNW sensor, both spring-shaped and straight SiNWs were transferred onto a single flexible PI substrate, as illustrated in Fig. 3(a). When the substrate was bent to a curvature radius of R = 50 mm, the spring-shaped SiNW accommodated the deformation by undergoing axial elongation enabled by its fixed-end configuration. In contrast, the straight SiNW fractured under the same bending condition, demonstrating its limited mechanical compliance.

Finite element analysis (FEA) was conducted using COMSOL Multiphysics to simulate the mechanical response of both geometries. The SiNWs were modeled as suspended structures with one end fixed, and axial strain applied at the other. As shown in Fig. 3(b), the spring-shaped SiNW subjected to 20% axial strain exhibited localized stress concentrations at the curved apexes (marked in red). The extracted stress distribution [Fig. 3(c)] revealed that these regions experienced stress levels 2–3 times higher than those in the sloped segments, in agreement with previous studies.[35]

Despite these local stress peaks, the maximum stress in the spring-shaped SiNW remained below 3 GPa, well within the reported fracture range for crystalline silicon (2–10 GPa).[41–43] In contrast, the straight SiNW experienced a peak stress of approximately 3.8 GPa at the fixed end under only 2% axial strain [Figs. 3(d) and 3(e)], indicating a much lower deformation tolerance. These findings clearly highlight the mechanical superiority of the spring-shaped design, making it more suitable for integration into flexible and wearable electronic systems that demand repeated and multidirectional strain accommodation.

04 November 2026 08:20:43

Published under an exclusive license by AIP Publishing

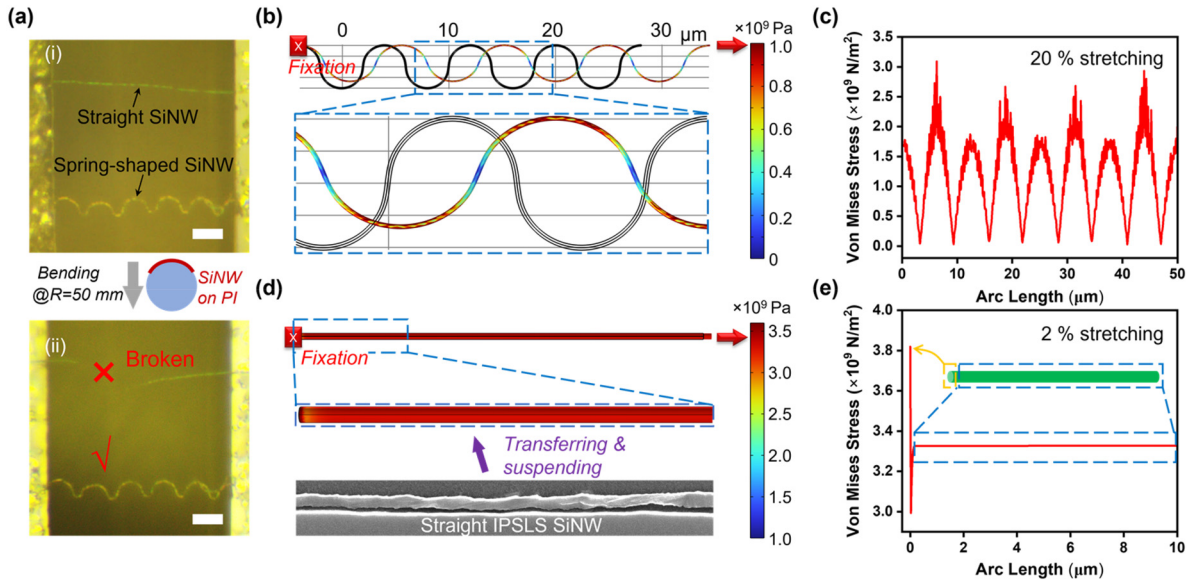


FIG. 3. Mechanical performance comparison between suspended spring-shaped and straight SiNWs. (a) Optical images of suspended spring-shaped and straight SiNWs before (i) and after (ii) bending deformation with a curvature radius of 50 mm. (b) Simulated stress distribution in a spring-shaped SiNW under 20% axial tensile strain. (c) Extracted stress profile along the arc length of the spring-shaped SiNW from (b). (d) Simulated stress distribution in a straight SiNW under 2% axial tensile strain. (e) Extracted stress profile along the arc length of the straight SiNW from (d). The scale bars in (a) represent 10 μm.

As a flexible and wearable strain sensor, the wind response performance of the spring-shaped SiNW-based device was systematically evaluated under simulated wearable conditions. To understand its mechanical behavior, we simulated the strain distribution of a suspended SiNW subjected to lateral deformation using COMSOL Multiphysics [Fig. 4(a)]. The corresponding strain values along the nanowire axis under different displacement levels are presented in Fig. 4(b). With both ends fixed, the maximum strain occurred at the midpoint during bending. The strain intensity increased proportionally with larger lateral displacements, reflecting the piezoresistive nature of the semiconductor SiNWs, where deformation leads to resistance modulation. In addition, the stress distribution under identical deformation conditions was analyzed [Figs. S1(a) and S1(b), supplementary material]. The results showed that stress levels increased with lateral displacement, while remaining below the fracture threshold of crystalline silicon across all tested conditions. These findings confirm the high mechanical robustness and stretchability of the SiNWs, making them well-suited for flexible sensing applications.

To assess the airflow sensing capability, a bent SiNW sensor (bending radius R = 50 mm) was exposed to a controlled airflow generated by a small fan, with the wind speed calibrated using a commercial anemometer [inset, Fig. 4(c)]. The I–V measurements revealed a significant current drop when the device was bent, with the current nearly 30-fold lower than that in the flat state (Fig. S2). As shown in Fig. 4(c), subsequent airflow exposure caused a further decrease in current, which progressively declined with increasing wind speed from 0.5 to 3 m/s. This current reduction arises from airflow-induced bending, which increases the strain and thereby the resistance, consistent with the typical response of p-type silicon.[36] Typical dynamic current responses at different airflow speeds are shown in Fig. 4(d). The current decreased progressively with increasing wind speed and recovered rapidly once the airflow ceased [Fig. 4(e)], demonstrating reversible behavior. The extracted calibration curve [Fig. 4(f)] exhibited excellent linearity ($R^2 = 0.996$) across three different devices, with additional results presented in Fig. S3, confirming the sensor's high sensitivity and reliability in airflow quantification. However, unlike substrate-bound structures, the strain experienced by suspended nanowires during bending is difficult to quantify accurately, making reliable extraction of the gauge factor [$GF = (\Delta R/R_0)/\varepsilon$] challenging. For comparison, the response curves of the same devices in the flat (unbent) state were also measured under identical airflow conditions. Although they also exhibited linear responses to varying wind speeds (Fig. S4), the magnitude of current change was significantly lower compared to the bent configuration.

Furthermore, the device demonstrated robust performance during continuous monitoring. When exposed to a constant airflow of 3 m/s for 5 s, the sensor produced stable and repeatable current signal changes [Figs. 4(g) and S5], with high relative current change ($\Delta I/I_0$) of 82%. A detailed analysis of the transient response [Fig. 4(h)] showed rapid response and recovery times of ~80 ms (defined as the time to reach 90% of the steady-state value), with statistical averages of 78.3 ± 5.4 and 78.3 ± 4.0 ms [Fig. 4(i)], respectively, outperforming most reported airflow sensors. Similarly, devices in the flat state (prior to bending) also exhibited continuous sensing capability and fast response/recovery times (~80 ms, Fig. S6), while their $\Delta I/I_0$ was relatively low (~50%). The bent sensors demonstrated excellent long-term stability after two months of ambient storage and robust durability under prolonged operation for over 5000 s (Figs. S7 and S8). Furthermore, they maintained stable performance and sensitivity under varying environmental temperatures and humidity levels (Figs. S9 and S10). These results highlight the unique advantage of spring-shaped SiNWs in sustaining reliable performance under mechanical deformation, representing a significant advancement for wearable airflow sensing technologies.

04 November 2026 08:20:43

Published under an exclusive license by AIP Publishing

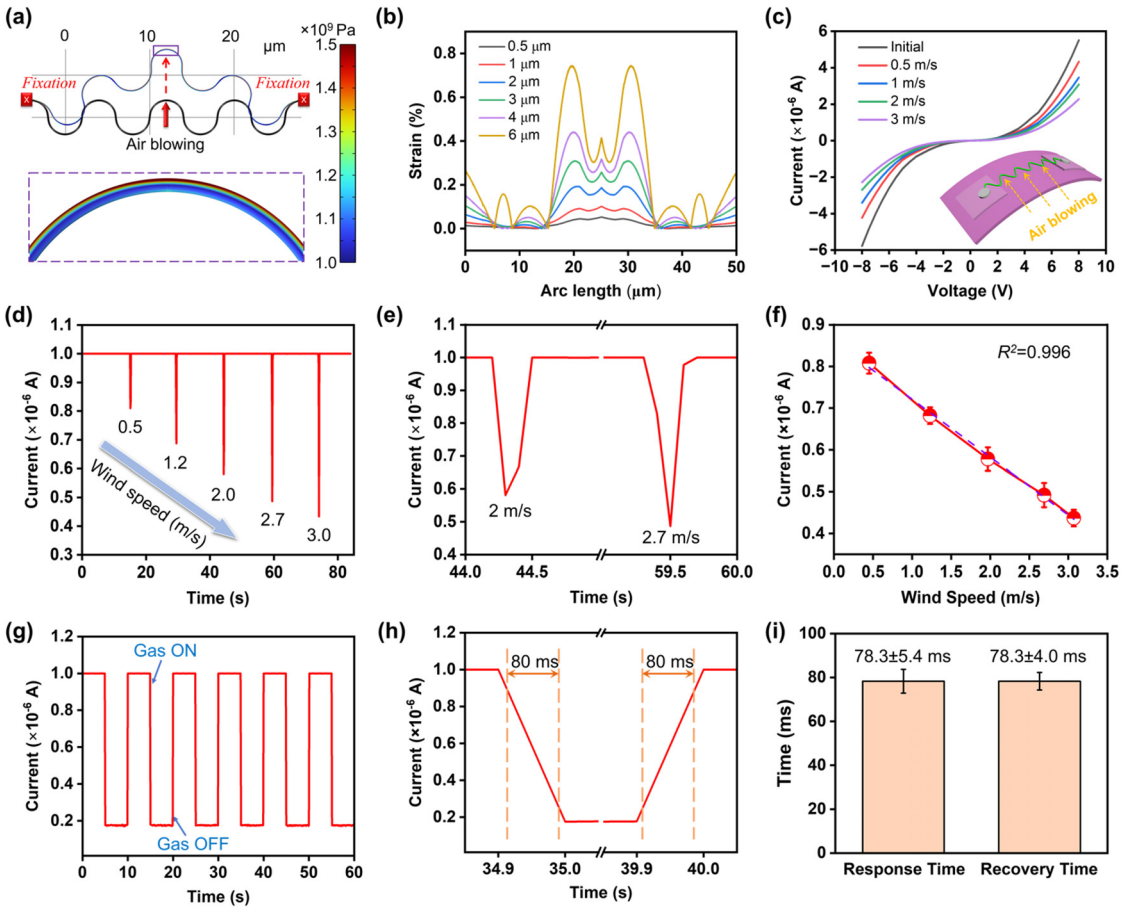


FIG. 4. Airflow sensing performance of the spring-shaped SiNW sensor. (a) Finite element simulation of the strain distribution along a suspended SiNW under a lateral displacement of 6 μm. (b) Extracted strain profiles along the nanowire under different displacement levels. (c) I–V characteristics of the bent SiNW sensor (bending radius R = 50 mm) at various airflow. Inset: schematic of the experimental airflow detection. (d) Real-time dynamic current response of the sensor to varying wind speeds. (e) Enlarged view of the response curves. (f) The plotted curve of current change as a function of wind speed ($n = 3$). (g) Continuous monitoring of airflow at a fixed wind speed (3 m/s). (h) Extracted response (~80 ms) and recovery (~80 ms) times from the transient curve in (g). (i) Statistical analysis of measured response and recovery times.

In real-world scenarios, airflow can originate from diverse angles and orientations, necessitating sensing devices capable of detecting strain variations in multiple directions. Leveraging their unique suspended and spring-shaped geometry, the SiNWs exhibit direction-dependent strain distributions when deformed under airflow from different directions. In this study, we systematically evaluated their multidirectional airflow sensing capabilities, focusing on three representative orientations: lateral (0°), oblique (45°), and top-down (90°), as illustrated in Fig. 5(a).

As shown in Figs. 5(b) and S11a, the sensor exhibited rapid and distinct current responses to airflow from all tested directions, demonstrating excellent directional sensitivity. Under a constant wind speed of 3 m/s, lateral airflow (0°) induced the largest current change $\Delta I/I_0$ (~56%), followed by the oblique direction (45°, ~38%), while top-down airflow (90°) produced the smallest response (~16%). The statistical analysis of the response is shown in Fig. S11(b). These results clearly indicate that the sensor's electrical output is strongly dependent on airflow direction.

To interpret the experimental trends, COMSOL simulations were conducted to model the strain distribution along the suspended SiNW under directional airflow, with an applied displacement of 3 μm [Fig. 5(c)]. The corresponding extracted strain profiles along the arc length [Fig. 5(d)] revealed that airflow from 0° induced the highest strain, while 90° airflow resulted in the lowest strain values, consistent with the observed piezoresistive current changes. Additional stress distribution analysis (Fig. S12) further supported these findings, showing a similar directional dependence. This anisotropic strain response, enabled by the spring-shaped design, offers a significant advantage over conventional straight SiNW sensors, which typically exhibit uniform responses regardless of airflow orientation. The demonstrated multidirectional sensitivity establishes a strong foundation for the development of advanced, high-resolution airflow disturbance sensors for wearable electronics and environmental monitoring applications. To further advance this platform toward practical use, future work will focus on improving the transfer yield and enabling large-scale array calibration under real-world conditions.

04 November 2026 08:20:43

Published under an exclusive license by AIP Publishing

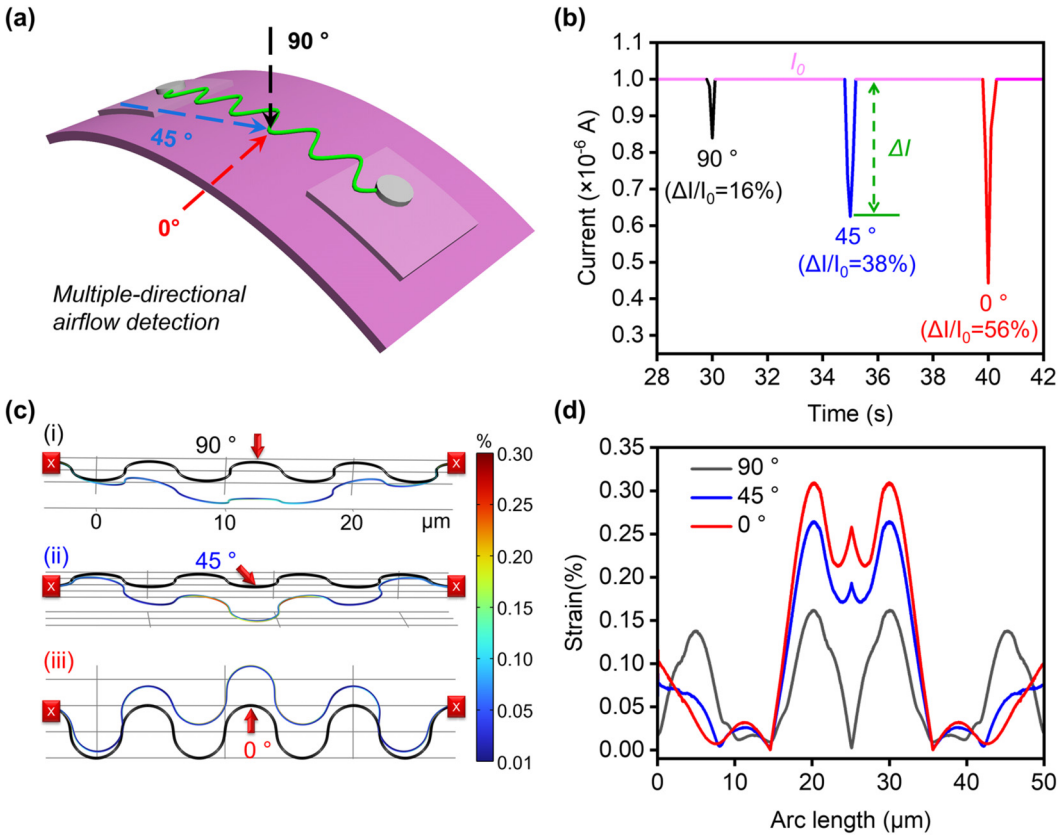


FIG. 5. Multidirectional airflow detection using the spring-shaped SiNW sensor. (a) Schematic illustration of the suspended spring-shaped SiNW sensor subjected to airflow from different directions: 0°, 45°, and 90°, relative to the sensor axis. (b) Measured current response curves under various airflow angles, demonstrating obviously directional sensitivity. (c) Simulated strain distribution along the suspended SiNW structure under three different airflow incidence angles. (d) Extracted strain profiles along the arc length of the spring-shaped SiNW corresponding to the simulations in (c).

In summary, we have developed a flexible and stretchable strain sensor based on suspended spring-shaped SiNWs, fabricated using IPSLS growth strategy. This structural innovation effectively overcomes the mechanical limitations and directional insensitivity of conventional straight SiNW-based sensors. By configuring the SiNWs into a spring-like geometry, the sensor exhibits excellent axial deformability and is well-suited for wearable applications involving frequent mechanical deformation. The suspended architecture minimizes substrate-induced constraints, enabling high, linear airflow sensitivity under bent conditions and a fast response time of 80 ms. Crucially, the spring-shaped configuration imparts direction-dependent strain sensitivity, allowing the sensor to detect multidirectional airflow, a capability not achievable with traditional straight SiNWs. This enhanced directional response significantly broadens the functional scope of SiNW-based sensors. Collectively, our findings establish a promising design framework for next-generation, high-performance, and multifunctional flexible sensors, with potential applications in environmental monitoring, wearable health diagnostics, and soft robotics.

See the supplementary material for more details on experimental methods and other characterization results.

The authors gratefully acknowledge financial support from the National Natural Science Foundation of China for Distinguished Young Scholars (Grant No. 62325403), the National Key Research Program of China (Grant No. 92164201), the National Natural Science Foundation of China (Grant No. 62104100), and the LvYangJinFeng Talent Program of Yangzhou and Postgraduate Research & Practice Innovation Program of Jiangsu Province (Grant No. SJCX25_2247).

AUTHOR DECLARATIONS

Conflict of Interest

The authors have no conflicts to disclose.

Author Contributions

Zongguang Liu: Conceptualization (lead); Funding acquisition (lead); Investigation (equal); Methodology (equal); Project administration (lead); Supervision (lead); Validation (equal); Visualization (equal); Writing – original draft (equal); Writing – review & editing (lead). **Haotian Wu:** Investigation (lead); Methodology (lead); Validation (equal); Visualization (equal); Writing – original draft (equal); Writing

04 November 2026 08:20:43

Published under an exclusive license by AIP Publishing

– review & editing (equal). **Hongyu Wu:** Formal analysis (equal); Investigation (equal); Methodology (equal); Writing – original draft (supporting); Writing – review & editing (equal). **Ruijin Hu:** Investigation (supporting); Methodology (supporting); Supervision (equal); Writing – original draft (equal); Writing – review & editing (supporting). **Shaobo Zhang:** Investigation (equal); Methodology (supporting); Supervision (equal); Validation (supporting); Writing – original draft (supporting); Writing – review & editing (equal). **Yunqing Cao:** Investigation (supporting); Methodology (equal); Validation (supporting); Writing – original draft (supporting); Writing – review & editing (supporting). **Junzhuan Wang:** Supervision (supporting); Validation (supporting); Writing – original draft (supporting); Writing – review & editing (supporting). **Kunji Chen:** Supervision (supporting); Validation (supporting); Writing – original draft (supporting); Writing – review & editing (supporting). **Jianmei Chen:** Conceptualization (equal); Investigation (equal); Methodology (equal); Resources (equal); Supervision (equal); Validation (lead); Visualization (lead); Writing – original draft (lead); Writing – review & editing (equal). **Linwei Yu:** Conceptualization (equal); Funding acquisition (equal); Project administration (equal); Resources (equal); Supervision (equal); Visualization (equal); Writing – original draft (supporting); Writing – review & editing (supporting).

DATA AVAILABILITY

The data that support the findings of this study are available within the article and its supplementary material.

REFERENCES

[1]K. Zhang, Z. Liu, Y. Zhou, Z. Li, D. Zhao, X. Guan, T. Lan, Y. Gong, B. Zhou, and J. Zhong, "Thin and flexible breeze-sense generators for non-contact haptic feedback in virtual reality," Nano-Micro Lett. **17**(1), 144 (2025).

[2]T. Liu, Q. Wu, H. Liu, X. Zhao, X. Yi, J. Liu, Z. Nong, B. Zhou, Q. Wang, and Z. Liu, "A crosslinked eutectogel for ultrasensitive pressure and temperature monitoring from nostril airflow," Nat. Commun. **16**(1), 3334 (2025).

[3]Q. Yu, Y. Zhang, L. Jiang, L. Li, X. Li, and J. Zhao, "Flexible optical fiber sensor for non-invasive continuous monitoring of human physiological signals," Small Methods **9**(4), 2401368 (2025).

[4]Q. Jiang, K. Leu, F. Wang, R. Li, K. Wang, Y. Zhao, A. Xi, Y. Zang, and R. Zhang, "Structural design and controlled fabrication of advanced airflow sensors," J. Mater. Chem. C **13**(10), 4876–4893 (2025).

[5]C. Xu, P. V. Nielsen, L. Liu, R. L. Jensen, and G. Gong, "Human exhalation characterization with the aid of schlieren imaging technique," Build. Environ. **112**, 190–199 (2017).

[6]H. Li, J. Wen, Z. Ou, E. Su, F. Xing, Y. Yang, Y. Sun, Z. L. Wang, and B. Chen, "Leaf-like TENGs for harvesting gentle wind energy at an air velocity as low as 0.2 m s^{-1}," Adv. Funct. Mater. **33**(11), 2212207 (2023).

[7]Z. Ren, Z. Wang, Z. Liu, L. Wang, H. Guo, L. Li, S. Li, X. Chen, W. Tang, and Z. L. Wang, "Energy harvesting from breeze wind (0.7–6 m s^{-1}) using ultra-stretchable triboelectric nanogenerator," Adv. Energy Mater. **10**(36), 2001770 (2020).

[8]S. Lee, S.-H. Bae, L. Lin, Y. Yang, C. Park, S.-W. Kim, S. N. Cha, H. Kim, Y. J. Park, and Z. L. Wang, "Super-flexible nanogenerator for energy harvesting from gentle wind and as an active deformation sensor," Adv. Funct. Mater. **23**(19), 2445–2449 (2013).

[9]M. Gong, C. Tu, X. Lin, F. Wang, H. Lian, Z. Cui, and X. Chen, "Liquid metal-graphene composite conductive nanofiber flexible pressure sensor for dynamic health monitoring," Mater. Des. **252**, 113811 (2025).

[10]Q. Jiang, R. Li, F. Wang, X. Shi, F. Chen, Y. Huang, B. Wang, W. Zhang, X. Wu, F. Wei, and R. Zhang, "Ultrasensitive airflow sensors based on suspended carbon nanotube networks," Adv. Mater. **34**(18), 2107062 (2022).

[11]X. Wu, Z. Zhang, H. Zhao, Y. Wang, J. Zhou, D. Meng, Y. He, M. Liu, Y. Zhang, Z. Xue, C. Jiang, M. Zhang, Z. Di, Y. Mei, and Q. Guo, "A skin-inspired optoelectromechanically coupled system for 3-axis airflow sensor," Nano Energy **135**, 110659 (2025).

[12]W. Zhou, P. Xiao, Y. Liang, Q. Wang, D. Liu, Q. Yang, J. Chen, Y. Nie, S. W. Kuo, and T. Chen, "Bionic adaptive thin-membranes sensory system based on microspring effect for high-sensitive airflow perception and noncontact manipulation," Adv. Funct. Mater. **31**(42), 2105323 (2021).

[13]S. Maharjan, V. K. Samoei, O. Amili, K. Sano, H. Honma, and A. H. Jayatissa, "Design and fabrication of a graphene/polyvinylidene fluoride nanocomposite-based airflow sensor," ACS Omega **7**(9), 7981–7988 (2022).

[14]T. Qi, C. Chen, Z. Yong, X. Gong, and S. Ramakrishna, "A robust bridge-type airflow sensor based on flexible superhydrophobic carbon nanotube fiber thin films," Adv. Mater. Interfaces **11**(1), 2300077 (2024).

[15]W. Wang, Z.-Q. Chen, Y.-Q. Li, Y.-L. Wang, M.-C. Liu, Y.-B. Ruan, Y. Zhang, S.-J. Liu, and Q. Zhao, "Laser direct writing of flexible multifunctional airflow sensors on the Kevlar fabric," Nano Res. **18**(1), 94907062 (2025).

[16]B. Yan, J. Wang, Y. Chen, Y. Li, X. Gao, Z. Hu, X. Zhou, M. Li, Z. Yang, and C. Zhang, "Ultra-sensitive micro thermoelectric device for energy harvesting and ultra-low airflow detection," Microsyst. Nanoeng. **11**(1), 73 (2025).

[17]H. Wang, S. Li, Y. Wang, H. Wang, X. Shen, M. Zhang, H. Lu, M. He, and Y. Zhang, "Bioinspired fluffy fabric with in situ grown carbon nanotubes for ultrasensitive wearable airflow sensor," Adv. Mater. **32**(11), 1908214 (2020).

[18]C. Shen, S. Sun, H. Zhang, and Z. Zhang, "Bioinspired ultrasensitive and flexible airflow sensor based on short carbon fiber network," Adv. Mater. Technol. **8**(1), 2200571 (2023).

[19]L. Huang, Y. Liu, G. Li, Y. Song, J. Su, L. Cheng, W. Guo, G. Zhao, H. Shen, Z. Yan, B. Z. Tang, and R. Ye, "Ultrasensitive, fast-responsive, directional airflow sensing by bioinspired suspended graphene fibers," Nano Lett. **23**(2), 597–605 (2023).

[20]J. S. Lee, K. W. Choi, J. Y. Yoo, M. S. Jo, and J. B. Yoon, "Realization of nanolene: A planar array of perfectly aligned, air-suspended nanowires," Small **16**(13), 1906845 (2020).

[21]R. He and P. Yang, "Giant piezoresistance effect in silicon nanowires," Nat. Nanotechnol. **1**(1), 42–46 (2006).

[22]K. Winkler, E. Bertagnolli, and A. Lugstein, "Origin of anomalous piezoresistive effects in VLS grown Si nanowires," Nano Lett. **15**(3), 1780–1785 (2015).

[23]B. Zhang, H. Wang, Y. Zhao, F. Li, X. Ou, B. Sun, and X. Zhang, "Large-scale assembly of highly sensitive Si-based flexible strain sensors for human motion monitoring," Nanoscale **8**(4), 2123–2128 (2016).

[24]B. Zhang, J. Yu, and X. Zhang, "A perspective on ultralong silicon nanowires for flexible sensors," Appl. Phys. Lett. **120**(13), 130501 (2022).

[25]S. Zhang, L. Lou, and C. Lee, "Piezoresistive silicon nanowire based nanoelectromechanical system cantilever air flow sensor," Appl. Phys. Lett. **100**(2), 023111 (2012).

[26]S. Huang, B. Zhang, Y. Lin, C. Lee, and X. Zhang, "Compact biomimetic hair sensors based on single silicon nanowires for ultrafast and highly-sensitive airflow detection," Nano Lett. **21**(11), 4684–4691 (2021).

[27]T. Kim, M. Lee, H. Ko, and D. I. Cho, "Piezoresistance of silicon nanowires for sensing applications: Optimizing nanowire parameters from electrical and mechanical perspectives," IEEE Access **12**, 99094–99109 (2024).

[28]J. Kim, M. Lee, H. J. Shim, R. Ghaffari, H. R. Cho, D. Son, Y. H. Jung, M. Soh, C. Choi, and S. Jung, "Stretchable silicon nanoribbon electronics for skin prosthesis," Nat. Commun. **5**(1), 5747 (2014).

[29]Y. Cui, L. J. Lauhon, M. S. Gudiksen, J. Wang, and C. M. J. A. P. L. Lieber, "Diameter-controlled synthesis of single-crystal silicon nanowires," Appl. Phys. Lett. **78**(15), 2214–2216 (2001).

[30]B. Zhang, H. Wang, L. He, C. Zheng, J. Jie, Y. Lifshitz, S. Lee, and X. Zhang, "Centimeter-long single-crystalline Si nanowires," Nano Lett. **17**(12), 7323–7329 (2017).

[31]S. Y. Ryu, J. Xiao, W. I. Park, K. S. Son, Y. Y. Huang, U. Paik, and J. A. Rogers, "Lateral buckling mechanics in silicon nanowires on elastomeric substrates," Nano Lett. **9**(9), 3214–3219 (2009).

[32]F. Xu, W. Lu, and Y. Zhu, "Controlled 3D buckling of silicon nanowires for stretchable electronics," ACS Nano **5**(1), 672–678 (2011).

[33]Z. Xue, M. Sun, T. Dong, Z. Tang, Y. Zhao, J. Wang, X. Wei, L. Yu, Q. Chen, J. Xu, Y. Shi, K. Chen, and P. Roca i Cabarrocas, "Deterministic line-shape programming of silicon nanowires for extremely stretchable springs and electronics," Nano Lett. **17**(12), 7638–7646 (2017).

04 November 2026 08:20:43

Published under an exclusive license by AIP Publishing

[34]T. Dong, Y. Sun, Z. Zhu, X. Wu, J. Wang, Y. Shi, J. Xu, K. Chen, and L. Yu, "Monolithic integration of silicon nanowire networks as a soft wafer for highly stretchable and transparent electronics," Nano Lett. **19**(9), 6235–6243 (2019).
[35]R. Yuan, W. Qian, Z. Liu, J. Wang, J. Xu, K. Chen, and L. Yu, "Designable integration of silicide nanowire springs as ultra-compact and stretchable electronic interconnections," Small **18**(6), 2104690 (2022).
[36]X. Song, Y. Gu, S. Wang, J. Fan, J. An, L. Yan, B. Sun, J. Wang, and L. Yu, "Scalable integration of high sensitivity strain sensors based on silicon nanowire spring array directly grown on flexible polyimide films," Nano Lett. **25**(6), 2290–2297 (2025).
[37]L. Yu, P.-J. Alet, G. Picardi, and P. Roca i Cabarrocas, "An in-plane solid-liquid-solid growth mode for self-avoiding lateral silicon nanowires," Phys. Rev. Lett. **102**(12), 125501 (2009).
[38]L. Yu and P. Roca i Cabarrocas, "Initial nucleation and growth of in-plane solid-liquid-solid silicon nanowires catalyzed by indium," Phys. Rev. B **80**(8), 085313 (2009).
[39]Y. Cheng, Z. Liu, J. Wang, J. Xu, and L. Yu, "Deterministic single-row-droplet catalyst formation for uniform growth integration of high-density silicon nanowires," ACS Appl. Mater. Interfaces **16**, 23625–23633 (2024).
[40]L. Liang, L. Wu, W. Liao, W. Qian, Y. Zhang, R. Hu, J. Wang, and L. Yu, "Performance improvement of planar silicon nanowire field effect transistors via catalyst atom doping control," J. Alloys Compd. **1001**, 175189 (2024).
[41]Z. Liu, J. Yan, H. Ma, T. Hu, J. Wang, Y. Shi, J. Xu, K. Chen, and L. Yu, "Ab initio design, shaping, and assembly of free-standing silicon nanoprobes," Nano Lett. **21**(7), 2773–2779 (2021).
[42]H. Zhang, J. Tersoff, S. Xu, H. Chen, Q. Zhang, K. Zhang, Y. Yang, C.-S. Lee, K.-N. Tu, J. Li, and Y. Lu, "Approaching the ideal elastic strain limit in silicon nanowires," Sci. Adv. **2**(8), e1501382 (2016).
[43]R. A. Minamisawa, M. J. Süess, R. Spolenak, J. Faist, C. David, J. Gobrecht, K. K. Bourdelle, and H. Sigg, "Top-down fabricated silicon nanowires under tensile elastic strain up to 4.5%," Nat. Commun. **3**(1), 1096 (2012).

04 November 2026 08:20:43

Published under an exclusive license by AIP Publishing